NANO EXPRESS

Magnetic Properties of Ni-doped ZnO Nanocombs by CVD Approach

Zhou ShaoMin · Yuan HongLei · Liu LiSheng · Chen XiLiang · Lou ShiYun · Hao YaoMing · Yuan RuiJian · Li Ning

Abstract The search for above room temperature ferromagnetism in dilute magnetic semiconductors has been intense in recent year. Arrays of perpendicular ferromagnetic nanowire/rods have recently attracted considerable interest for their potential use in many areas of advanced nanotechnology. We report a simple low-temperature chemical vapor deposition (CVD) to create self-assembled comb-like Ni-/undoped ZnO nanostructure arrays. The phases, compositions, and physical properties of the studied samples were analyzed by different techniques, including high-resolution X-ray diffraction/photoelectron spectroscopy/transmission electron microscopy, photoluminescence, and MPMS. In particular, the Ni-doped ZnO nanocombs (NCs) with ferromagnetic and superparamagnetic properties have been observed whereas undoped ZnO NCs disappear. The corresponding ferromagnetic source mechanism is discussed, in which defects such as O vacancies would play an important role.

Keywords Magnetism · II–VI semiconductors · Nanostructures · Zinc oxide

Introduction

An array of hierarchical assembly of nanoscale building blocks such as nanocomb/cantilevers (NCs) is a crucial step toward realization of functional nanosystems and represents a significant challenge in the field of nanoscale science [1–5]. Dilute magnetic semiconductors (DMSs) are attracting intense interest for potential new device applications in spin-based information-processing technologies [6–22]. The development of practical semiconductor spintronic devices will require new DMSs with Curie temperature above room temperature [6–21]. Therefore, DMSs of above room temperature ferromagnetism (ARTF) doping NCs provide a very good opportunity to integrate new functionality into the existing semiconductor nanodevices [6]. Ni is an excellent resistance to corrosion, ferromagnetic, and reasonable conductor of heat and electricity. In addition, ion radius of Ni (~ 0.69 Å) is smaller than that of Zn (~ 0.74 Å) and the ZnO compound can be easily substituted by Ni^{2+}. Motivated by this approach, possibly, Ni ions substitute part of Zn^{2+} in ZnO, which turn ZnO nanoparticles into Ni-doped ZnO NCs based on a vapor chemical reaction. Recently, room temperature magnetic properties of Ni-doped ZnO simple nanostructures such as nanoparticles and nanowire/rods have widely been reported [11–20]. To date, however, ARTF Ni-doped ZnO hierarchical nanostructures such as NCs have not been limited though ferromagnetism of Co-doped ZnO nanoarrays has been reported by our research group [6]. Previously, we have studied on the fabrication of Ni-doped ZnO NCs and investigated their optical properties [3]. In this paper, we systematically researched on their magnetic and optical properties, which reveal that the as-studied Ni-doped ZnO NC samples exhibit ARTF behaviors with saturation magnetization of 0.62 emu/g and coercivity value up to 88 Oe, as well as, the ferromagnetic ordering in Ni-doped ZnO NCs is very sensitive to the annealing temperature.

Z. ShaoMin (✉) · Y. HongLei · L. LiSheng · C. XiLiang · L. ShiYun · H. YaoMing · Y. RuiJian · L. Ning
Key Lab for Special Functional Materials of Ministry of Education, Henan University, 475004 Kaifeng, People's Republic of China
e-mail: smzhou@henu.edu.cn

Experimental Section

Samples of un/Ni-doped ZnO NCs were synthesized on Si substrates in a horizontal tube furnace system, which is similar to our earlier reports [2–4, 6]. In a typical process, a solution of nickel nitrate (nominal rate: 0, 0.1, or 0.2 M) and ethanol was dropped onto the Si substrate. After drying the Si substrate at 373 K in ambient air (to form uniform $Ni(NO_3)_2$ film), some particles were evenly formed on the Si substrate. Then, the substrate was put on the top of a quartz boat loaded with commercial zinc powders (5.0 g, 99.999%) and inserted into a quartz tube furnace. The zinc source was physically vaporized to chemically synthesize the $Zn_{1-x}Ni_xO$ ($x = 0, 0.1, 0.2$) samples in atmospheric pressure under N_2 (99.999%) flow rate of 50 sccm for 120 min at the temperature of 723 K. After the reaction, the substrate surface appeared as a layer of wax-like material. The morphologies and microstructure/compositions of these as-fabricated specimens were investigated by scanning/transmission electron microscopy (SEM/TEM, XL 30-S-FEG/JEOL 2010), selected area electron diffraction (SAED), the energy dispersive X-ray spectroscopy (EDS), and high-resolution (HR) TEM (HRTEM). The bulk crystal structures and chemical constitutions were detected by HR X-ray diffraction/photoelectron spectroscopy [HRXRD/HRXPS (X'pert MRD-Philips diffractometer with Cu K_α radiation, $\lambda = 0.154056$ nm)/(MKII XPS, Mg $K\alpha$)], and inductively coupled plasma spectrometer (ICP-96B), respectively. Room temperature photoluminescence (RTPL) measurements were carried out by a fluorescence spectrophotometer (SPEX F212) with as the excitation light source (330 nm). Magnetic properties were carried out by using Quantum Design Superconductor Quantum Interference Device (SQUID) (MPMS XL5) at temperatures from 5 to 400 K with the applied magnetic field perpendicular or parallel (500 Oe, in-plane or out-plane) to the studied bulk specimens.

Results and Discussion

A typical SEM image of the $Zn_{0.8}Ni_{0.2}O$ sample is shown in Fig. 1a, which reveals that the as-obtained products are composed of large quantities of high-quality comb-like nanostructures with the typical length up to several ten microns. In fact, the morphologies and sizes of the others ($Zn_{0.9}Ni_{0.1}O$ and ZnO specimens) are similar to those of 20%-Ni-doped ZnO NCs (not shown). A representative wide-scan (20°–80°) XRD pattern (not revealed) contains HRXRD spectra to indicate a hexagonal wurtzite-structured ZnO. Figure 1b shows three explored HRXRD patterns, taken from the (002) spacing of $Zn_{0.8}Ni_{0.2}O$, $Zn_{0.9}Ni_{0.1}O$, and ZnO NCs, respectively. Both of the (002)
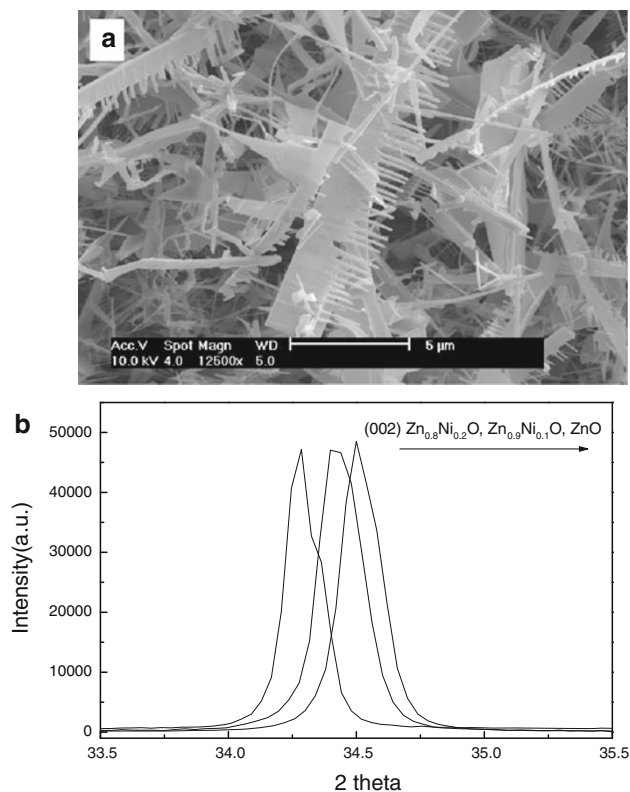

Fig. 1 A typical low amplification SEM image (**a**) of $Zn_{0.8}Ni_{0.2}O$ NCs; Three HRXRD patterns (002) (**b**) from $Zn_{0.8}Ni_{0.2}O$ NCs, $Zn_{0.9}Ni_{0.1}O$ NCs, and ZnO NCs

diffraction peaks of Ni-doped NCs have a slight shift to low two theta angle compared with undoped NCs. Unlike our earlier report [3], $Zn_{0.8}Ni_{0.2}O$ NCs formed in the work shift the peak position to a low angle relative to the undoped ZnO (about 0.21°). The reason may be different doping types from dissimilar conditions, including the low temperature chemical reaction and gas glow, as well as a lot of distortions in the host ZnO lattices.

A representative HRSEM image of the $Zn_{0.8}Ni_{0.2}O$ is shown in Fig. 2a. It can be seen that all nanorod branches have uniform diameters and are evenly distributed at only one side of the stem with a periodicity of 150–250 nm. In addition, diameter and length of the branched chains are about 50–80 nm and ~ 1 μm, respectively. As shown Fig. 2b, a corresponding low enlargement TEM image of $Zn_{0.8}Ni_{0.2}O$ is demonstrated. It is more obvious that the products have array morphology, uniform diameter, and periodic structures, which are excellent in agreement on these results taken from SEM images. These hierarchically ordered nanowire/rod arrays are monolithically single crystalline as evidenced by the SAED pattern and HRTEM as exposed in two inset images of Fig. 2b. The SAED model (right inset) shows that the as-synthesized sample is indexed to a hexagonal wurtzite phase and the comb backbone grows along [$2\bar{1}\bar{1}0$], its top/bottom surfaces are
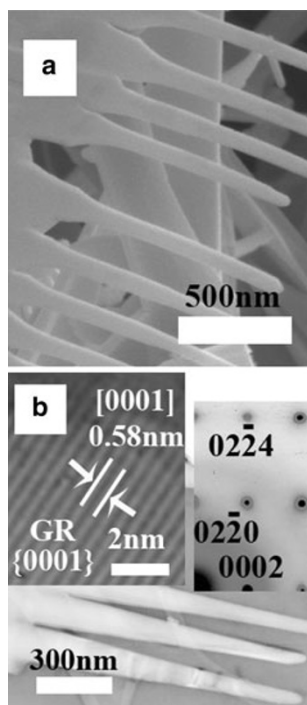
Fig. 2 HRSEM image (**a**) and TEM image (**b**) for $Zn_{0.8}Ni_{0.2}O$ (*left inset*: SAED, *right one*: HRTEM)

$(01\bar{1}0)$, and the nanobranches grow along [0001] direction. HRTEM was applied to image microstructures of a single branch as shown in the left inset of Fig. 2b. In the HRTEM image, perfect and continuous lattice fringes disclose that Ni^{2+} ions were averagely adulterated into the crystal lattice of ZnO and formed a single crystal structure with hexagonal phase, which is compatible with results of XRD and SAED. Based on calculations of HRTEM, SAED, and XRD, the lattice spacing (0001) of Ni-doped NCs (0.58 nm) is a little larger than that of undoped ZnO sample (0.52 nm) [1], which is induced by doped Ni^{2+} ion into Zn^{2+} site. ICP analyses were carried out to obtain the contents of Zn, O, and Ni in the bulk samples. Data (not shown) confirm 3 M ratios of three kinds of samples are 80.4:19.6:98.6 ($Zn_{0.8}Ni_{0.2}O$), 90.1:9.9:98.8 ($Zn_{0.9}Ni_{0.1}O$), and 50.1:49.9 (ZnO), respectively, which are almost equal to their nominal compositions. In addition, HRXPS spectra of the bulk NCs ($Zn_{0.8}Ni_{0.2}O$) were shown in Fig. 3a, b. Based on peaks of Zn (1021.9 eV, 2p3/2) and Ni 2p3/2 (853.7 eV, 2p3/2), and their integral areas, the products must contain a small amount (up to ∼20%) Ni element. For single $Zn_{0.8}Ni_{0.2}O$ NCs, EDS was used to confirm its microcomposition as shown in Fig. 3c. It can be clearly seen that every NC has almost the same composition and contains a small amount of Ni. Further quantitative analysis finds that the atomic ratio between Zn and Ni is about 80.4:19.6, which is compatible with the data of IPC and HRXPS.
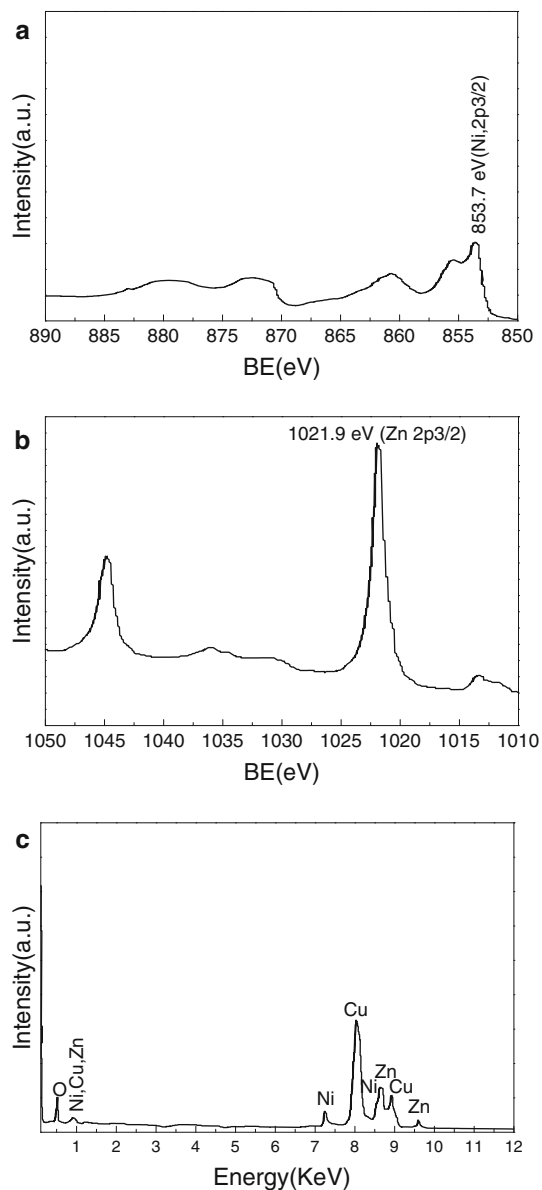

Fig. 3 HRXPS spectra [Ni 2p (**a**); Zn 2p (**b**)] and EDS pattern (**c**) of $Zn_{0.8}Ni_{0.2}O$ NCs

ZnNiO or ZnO could be simply formed by a chemical reaction; however, the formation of NCs would involve a very complicated process. Because of the fact that the NCs can only be formed at lower temperature region, we may speculate the NC formation procedure as follows: (1) the nucleation and growth along $[2\bar{1}\bar{1}0]$ forms the comb-stems; (2) slower growth along [0001] direction by a faceted epitaxial growth process creates the branched chain. Possibly, it is related to the supersaturated environments, and a great deal of Zn vapor exists in the reaction chamber, which grows ZnNiO or ZnO nucleation with O_2. Then, nucleation occurs as sites of ZnNiO or ZnO nanoparticles. Continuous feeding of an evaporated [(Zn + little Ni^{2+}) or

Zn] source and elemental oxygen would lead to form wire-/rod-like array (hierarchical) nanostructure (mainly from eutectoid of ZnNiO or ZnO). The more detailed growth mechanism was reported in our earlier papers [2–4, 6].

RTPL measurements were carried out by using the Xe lamp with an excitation wavelength of 330 nm. After annealing at different temperatures [873 K (blue, named for sample 1), 973 K (red, sample 2), 1,073 K (black, sample 3)] in Ar gas, RTPL spectra from a bulk quantity of $Zn_{0.8}Ni_{0.2}O$ NCs are shown in Fig. 4a. There are two obvious PL regions for the three different annealing temperatures. It is found that the strongest ultraviolet (UV) emission peak centered at about 3.27 eV (~ 379 nm) and a weakest broad green one band centered at ~ 2.46 eV (~ 504 nm) are from sample 1. Further annealed, however, the green emission peaks happen into magnification intensity whereas counterparts of UV emissions are decreasing. For example, the green peak of sample 3 is the highest while the UV emission changes into the weaker. The UV peak of ZnO is generally attributed to a recombination of free excitons, namely a near-band-edge transition of wide band gap of ZnO, and the green emission is thought that originates from the recombination of the holes with the electrons occupying the singly ionized oxygen vacancy [3–6, 11–21]. After samples are annealed at high temperatures, the excess carriers supplied by the impurities to the conduction band contribute to decrease the electrical conductivity of ZnO. The intensity of the green emission increases strongly, which means that the oxygen vacancy concentration in Ni-doped ZnO NCs increases after annealing at high temperatures [12, 15, 16, 18]. It is reasonable because oxygen atoms are easily evaporated during the higher temperature, especially in Ar ambient [21].

M-T properties were characterized by using quantum design SQUID magnetometer equipped with 5 T magnet in the temperature range 5–400 K. Since the NCs are the hierarchical aligned structures, it is natural to expect that the samples should show the perpendicular anisotropy, i.e., the magnetization prefers to be perpendicular to the NCs. In order to characterize the macroscopic anisotropy of the sample which is an average anisotropy of the individual NCs, the magnetic field, H has been applied perpendicular to and parallel to the NCs (Si wafer for the substrate). For our experiment, however, no significant difference has been observed in the two directions. The saturation magnetization and coercive field was found to be the same for the two directions within the experimental resolution, which is compatible with our previous report [6]. Figure 4b shows magnetization of sample 3 as a function of temperature obtained at the zero-field-cooled (ZFC) and field cooled (FC) processes with a small applied magnetic field of 500 Oe. It is evident that the $Zn_{0.8}Ni_{0.2}O$ NCs have ferromagnetically with Curie temperature higher than

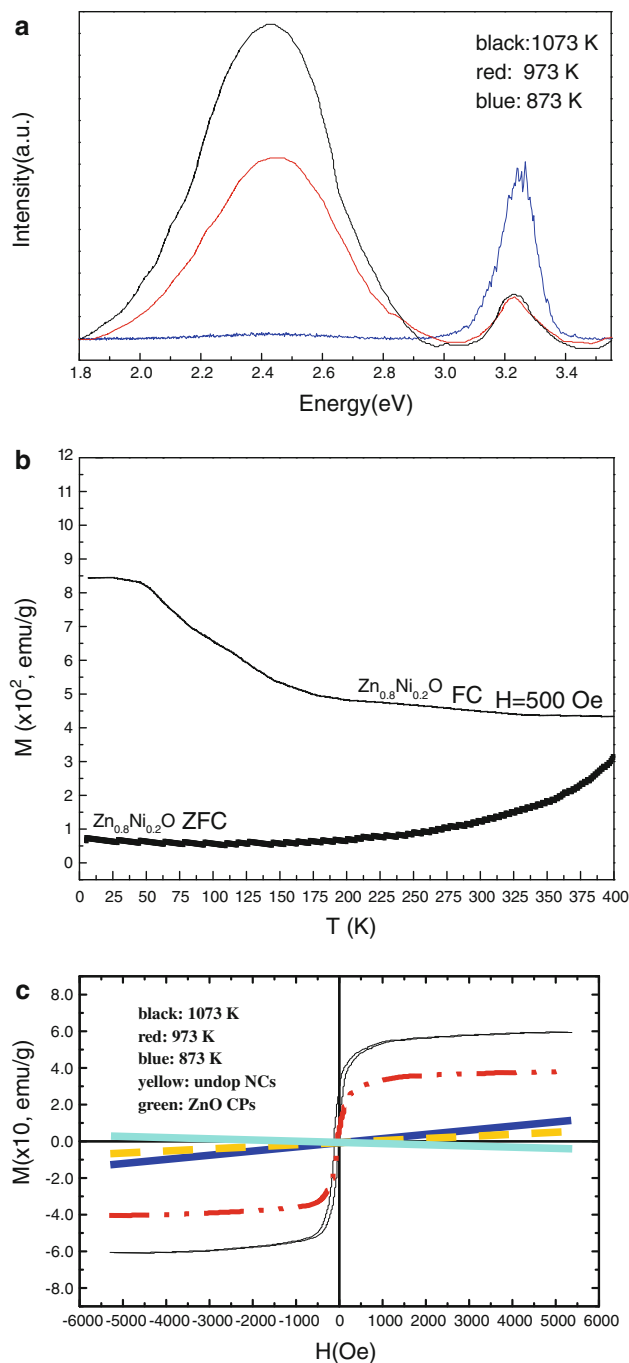**Fig. 4** Three RTPL spectra (**a**) of sample 1 (*blue*), 2 (*red*), and 3 (*black*); The magnetization as a function of temperature (**b**) for FC and ZFC [taken from sample 3]; RT M-H (**c**) of sample 1, 2, and 3, as well as undoped NCs and CPs annealed only at 1,073 K

400 K due to the clear separation between the FC and ZFC. The ZFC–FC magnetization curves clearly indicate that the sample is quite thermally stable without blocking (or superparamagnetic behavior), which is similar to earlier reports on Ni-doped nanostructures [11–20]. In addition, Fig. 4c is presented for RT M-H properties of sample (1, 2, and 3), as well as both of undoped NCs and conventional

powders (CPs) (both of them were annealed only at 1,073 K). It can be clearly seen that the highest temperature annealing $Zn_{0.8}Ni_{0.2}O$ NCs have a saturation magnetization (M_s, ∼ 0.62 emu/g) and coercivity value (H_c) amounts to about 88 Oe, which are more than $Zn_{0.95}Ni_{0.05}O$ nanorods (M_s: 0.4 emu/g, H_c: 72 Oe) [17]. As for sample 2, however, the studied $Zn_{0.8}Ni_{0.2}O$ NCs exhibit a RT superparamagnetic behavior, in which no coercivity or remanence is observed. However, both of the undoped ZnO NCs and sample 3 are paramagnetic properties whereas CPs have a diamagnetic behavior, which is partly compatible with previous report [22]. As to the origin of ferromagnetic behavior observed in Ni-doped ZnO nanostructures, there are a few of controversial explanations, one of which is the formation of some nanoscale Ni-related secondary phase, such as metallic Ni precipitation and NiO. In fact, however, NiO phase can be easily ruled out, since bulk NiO is antiferromagnetism with a Neel temperature of 520 K [17]. Secondly, based on our experimental conditions, metallic Ni is also an unlikely source of this ferromagnetism because the synthesis of Ni-doped ZnO NCs is performed in air which can prevent the formation of metallic Ni nanoclusters to some extent. In addition, XRD and HRTEM results clearly show no metallic Ni clusters in the NCs. According to the optical and magnetic data, one can see that it is apparent that the ferromagnetic properties of $Zn_{0.8}Ni_{0.2}O$ NCs have a strong correlation with oxygen vacancies, which is compatible with earlier literatures [6, 11–21]. Of course, convincing explanation on the relation of ARTF is our further work.

Conclusion

To summarize, ARTF and RT superparamagnetic behaviors of Ni-doped ZnO NCs have firstly been observed after heat treating. The present study not only demonstrates Ni-doped ZnO NCs emit green light but also suggests that introducing oxygen vacancies is an effective way to boost the ARTF. In addition, Ni-doped ZnO NCs have been fabricated by using a simple chemical vapor-deposition method, in which the process is friendly environment. Such doping hierarchical nanostructures with carefully tailored composition may find potential applications in high-density data storage and other magnetic/semiconducting-device applications.

References

1. Z. Wang, X. Kong, J. Zuo, Phys. Rev. Lett. **91**, 185502 (2003)
2. S. Zhou, X. Meng, X. Zhang, X. Fan, K. Zou, S. Wu, S. Lee, Micron **36**, 55 (2005)
3. B. Zhang, X. Zhang, H. Gong, Z. Wu, S. Zhou, Z. Du, Phys. Lett. A **372**, 2300 (2008)
4. B. Zhang, S. Zhou, H. Wang, Z. Du, Chinese Sci. Bull. **53**, 1639 (2008)
5. Q. Ahsanulhaq, J. Kim, J.H. Kim, Y. Hahn, Nanosc. Res. Lett. **5**, 669 (2010)
6. S. Zhou, P. Wang, S. Li, B. Zhang, H. Gong, L. Du, Chinese Phys. Lett. **25**, 4446 (2008)
7. P. Sharma, A. Gupta, K. Rao, F. Owens, R. Sharma, R. Ahuja, J. Guillen, B. Johansson, G. Gehring, Nat. Mater. **2**, 673 (2003)
8. J. Coey, M. Venkatesan, C. Fitzgerald, Nat. Mater. **4**, 173 (2005)
9. F. Owens, Nanosc. Res. Lett. **2**, 447 (2007)
10. R. Sanz, J. Jensen, G. Gonzalez, O. Martinez, M. Vazquez, M. Hernandez-Velez, Nanosc. Res. Lett. **4**, 878 (2009)
11. C. Cong, J. Hong, Q. Liu, L. Liao, K. Zhang, Solid State Commun. **138**, 511 (2006)
12. H. Wang, Y. Chen, H. Wang, C. Zhang, F. Yang, J. Duan, C. Yang, Y. Xu, M. Zhou, Q. Li, Appl. Phys. Lett. **90**, 052505 (2007)
13. G. Huang, J. Wang, X. Zhong, G. Zhou, H. Yan, J. Mater. Sci. **42**, 6464 (2007)
14. M. El-Hilo, A. Dakhel, A. Ali-Mohamed, J. Magn. Magn. Mater. **321**, 2279 (2009)
15. J. Cui, U. Gibson, Appl. Phys. Lett. **87**, 133108 (2005)
16. J. Iqbal, B. Wang, X. Liu, D. Yu, B. He, R. Yu, New J. Phys. **11**, 063009 (2009)
17. C. Cheng, G. Xu, H. Zhang, Y. Luo, Mater. Lett. **62**, 1617 (2008)
18. X. Huang, G. Li, B. Cao, M. Wang, C. Hao, J. Phys. Chem. C **113**, 4381 (2009)
19. H. Shi, Y. Duan, Nanosc. Res. Lett. **4**, 480 (2009)
20. G. Xing, D. Wang, J. Yi, L. Yang, M. Gao, M. He, J. Yang, J. Ding, T. Sum, T. Wu, Appl. Phys. Lett. **96**, 112511 (2010)
21. H. Hsu, J. Huang, Y. Huang, Y. Liao, M. Lin, C. Lee, J. Lee, S. Chen, L. Lai, C. Liu, Appl. Phys. Lett. **88**, 242507 (2006)
22. Q. Xu, S. Zhou, H. Schmidt, J. Alloys Compd. **487**, 665 (2009)